Magnetic properties of cobalt and cobalt–platinum nanocrystals investigated by magneto-optical Kerr effect

C. Petit[a)]
Laboratoire des Matériaux Mésoscopiques et Nanométriques, UMR CNRS 7070, Université Pierre et Marie Curie, 4 Place Jussieu 75251 Paris Cedex, France

S. Rusponi and H. Brune
Institut de Physique des Nanostructures, Ecole Polytechnique Fédérale de Lausanne, PHB Ecublens CH-1015 Lausanne, Switzerland

(Received 8 July 2003; accepted 23 January 2004)

Magneto-optical Kerr effect, is used to investigate the magnetization of film made of uncoalesced cobalt and cobalt–platinum nanocrystals. For the pure cobalt nanocrystals, different film morphologies are obtained through application of magnetic field during deposition. These morphologies have quite different magnetic properties, which is rationalized by considering dipolar interactions and the associated demagnetizing factor. We show that *fast* annealing can be used to trigger changes in the particles' crystalline structure while largely avoiding their coalescence. With increasing the annealing temperature, 2.7 nm CoPt nanocrystals show a transition from the magnetically soft face-centered-cubic phase to the hard face-centered-tetragonal $L1_0$ phase. In particular *fast* annealing to 950 K is shown to produce largely uncoalesced nanocrystals ferromagnetic at room temperature. With 7 nm cobalt nanocrystals, *fast* annealing at 500 K equally results in ferromagnetism at room temperature without inducing coalescence between the nanocrystals in the film. © *2004 American Institute of Physics.* [DOI: 10.1063/1.1686906]

I. INTRODUCTION

Nanometer-sized magnetic particles have been attracting an ever growing interest over the last decades. Their properties differ considerably from those of the corresponding bulk materials due to the large fraction of the constituent atoms residing on the particle surface.[1] From a technological point of view ferromagnetic nanoparticles are potential candidates as fundamental constituents of future magnetic storage media.[2] In the ideal case of monodisperse magnetic anisotropy energy and aligned easy axes, a bit can be made by a single ferromagnetic particle.[3] However, there are several problems remaining to be solved before application in storage industry becomes feasible. Devices based on magnetic nanocrystals are limited by thermal fluctuations of the magnetization: due to their reduced sizes, ferromagnetic nanocrystals become superparamagnetic at room temperature. The dipolar magnetic interaction between nanocrystals ordered in arrays is also an important limiting factor for their use in magnetic storage media. A detailed understanding of the magnetic properties of assemblies of nanocrystals is therefore essential to the development of the magnetic recording technology. Many investigations have been made with cobalt nanocrystals.[4–6] Most of this work was devoted to studying the magnetic interactions between the particles.[7,8] Collective effects due to the dipolar interactions[9–11] or to the structure of the organization[12] have been pointed out in mesoscopic organizations. Despite their interest, studies of the optical and magneto-optical properties of ferromagnetic nanoparticles are scarce.[13–16] Only recently Kalska *et al.*[17] reported magneto-optics at room temperature of self-organized cobalt nanocrystals deposited on silica. However, to date none of these organizations of ferromagnetic nanocrystals can be used at room temperature. One way to overcome this limitation is the use of nanoalloys such as FePt[18,19] or CoPt,[20] because these magnetically hard materials have very high coercivity and can better resist the superparamagnetic effect.[21]

Colloidal chemistry is particularly appropriate for the synthesis of metallic nanocrystals as well as magnetic oxides of different size and composition.[22–24] Numerous studies deal with silver, gold, or semiconductor nanocrystals. Recently the synthesis of ferromagnetic nanocrystals based on $3d$ elements has been reported.[4,8] However, little work has been done on soft chemistry processes for the fabrication of such ferromagnetic nanocrystals[24] and there are only few reports on soft chemistry synthesis of nanoalloys such as CoPt.[25–27] Usually, the high temperature decomposition of organo-metallic compounds is used to form such nanoalloys.[6,28–31]

In this article, we investigate by magneto-optical Kerr effect (MOKE), the magnetic properties of various organizations of colloidal cobalt and CoPt nanoparticles deposited on highly ordered pyrolytic graphite (HOPG) substrates. The particles, synthesized by micellar route, have diameters of 7 and 2.7 nm for Co and $Co_{53}Pt_{47}$ nanocrystals, respectively. As grown the nanoparticles are superparamagnetic at room temperature. The effect of a *fast* thermal annealing under high vacuum on the particle magnetic anisotropy was analyzed in detail. Compared to the usual annealing procedure requiring some hours, *fast* annealing reduces coalescence be-

[a)]Author to whom correspondence should be addressed; electronic mail: petit@sri.jussieu.fr

low the detection limit. Our MOKE data demonstrate that 7 nm pure cobalt nanocrystals become ferromagnetic at room temperature upon a *fast* annealing to 500 K; 2.7 nm CoPt nanocrystals after *fast* annealing to 950 K equally show ferromagnetic behavior at room temperature. Our data suggest the absence or at least limited particle coalescence and thus we attribute the change in the magnetic properties to a transition from the magnetically soft face-centered-cubic (fcc) phase to the harder face-centered-tetragonal (fct) phase.

The second aspect we investigate in this article is the effect of the mesoscopic film morphologies on the interaction between the nanocrystals. Great progress has been achieved in the fabrication of colloid nanoparticle superlattice assemblies.[24,32] Nevertheless, the impossibility of controlling the particle orientation during film growth is still an unresolved issue. This point is of particular relevance in the case of ferromagnetic nanoparticles since it means the impossibility of controlling the orientation of the particle magnetization easy axis, a key issue to be solved for future application in data storage.[33] Recently, organizations of ferromagnetic nanoparticles have been obtained by applying an external magnetic field during growth.[10,11] Due to its reduced size, each ferromagnetic nanoparticle supports a single magnetic domain and can therefore be viewed as a constant magnetic moment. This macrospin may partly orientate along an external field applied during film deposition leading to a net stray field. This field favors specific sites and orientations of the subsequently deposited particles. As a consequence the film morphology made of uncoalesced cobalt nanocrystals reflects the symmetry imposed by the external magnetic field: in-plane stripes, conic mountains, or homogeneous flat films occur when an external field is applied in the film plane, perpendicular to it, or in zero field, respectively. Our MOKE data show different magnetic behavior due to the dipolar interactions between adjacent nanocrystals and to a partial orientation of the macrospin.

II. APPARATUS

Transmission Electron Microscopy (TEM). A JEOL (100 kV) model JEM 100CX II was used to obtain micrographs of the nanocrystals on amorphous carbon or HOPG-coated TEM grids.

Magnetic Properties. The magnetic measurements were made with a commercial superconducting quantum interference device (SQUID) magnetometer from SPEC (Cryogenic S600, CEA-Saclay, France).

Atomic Force Microscopy (AFM). A Park Scientific Instruments AUTOPROBE CP microscope was used in noncontact mode to obtain the topography of the nanocrystals deposited on HOPG substrates.

Moke Apparatus: Magneto-optical Kerr effect experiments were performed in a homemade UHV chamber. The Kerr setup, optimized to have submonolayer sensibility, comprises a temperature stabilized (± 0.1 K) 670 nm laser diode, two polarizers, and a photodetector. The light passes trough the first polarizer, a UHV window (with small birefringence) and then it impinges onto the sample with an incident angle of 30° with respect to the surface normal. The photodetector measures the intensity of the reflected light transmitted through a second UHV window and the second polarizer (analyzer). Kerr loops are measured with the analyzer set to about 1° from maximum extinction. In this configuration the light intensity is recorded to yield the magnetization as a function of the applied field. Using an electromagnet inside the UHV chamber, a magnetic field up to 500 Oe is created at the sample location, perpendicular to the sample plane (polar Kerr effect). The field sweep and the acquisition of the MOKE signal from the detector are computer controlled. The sample ($5\times 5\ \mathrm{mm}^2$) can be cooled down through a copper braid connected to the cold finger of a helium flux cryostat. The sample temperature is measured with a thermocouple in direct contact with the sample. Temperature stabilization is achieved by heating the sample via a radiating filament placed at less than 1 mm from the back of the sample. A voltage difference can be applied between sample and filament allowing sample heating by electron bombardment. In a typical *fast* annealing process, the temperature is increased with a rate of 10–20 K/s to the annealing value, where it is kept constant (within ± 0.1 K) at that value for the desired time (10 min for all the samples described in the article) and then quickly reduced to room temperature with a rate of 5–10 K/s. The temperature is controlled with an accuracy of ± 0.1 K in the range 50–2000 K. Altogether, this allows *fast* and controlled annealing of the sample. For the MOKE experiments, the HOPG substrate supporting the nanocrystals is glued to a copper holder by using conductive acrylic glue and heated at 370 K for 1 h under argon in order to assure the adhesion of the sample.

III. SYNTHESIS AND CHARACTERIZATION OF THE NANOCRYSTALS

A. Cobalt nanocrystals

The synthesis of 7-nm-diam cobalt nanocrystals in colloidal assemblies has been reported previously.[34] The particles are characterized by extended x-ray absorption fine structure spectroscopy and x-ray diffraction[4,34] showing the formation of pure cobalt nanocrystals. The nanocrystals are passivated by lauric acid, $CH_3(CH_2)_{10}COOH$, and are easily dispersed in a solvent like hexane. The polydispersity is relatively large with a half width at half maximum of the diameter distribution of $\sigma = 15\%$. When deposited on a substrate at low concentration, cobalt nanocrystals form a monolayer with well organized surface areas [Fig. 1(A)].

B. Cobalt–platinum nanocrystals

CoPt nanocrystals are synthesized in colloidal assemblies by a slight modification of the previous chemical process. They are prepared *in situ* in sodium di (ethylhexyl)sulfosuccinate (AOT) reverse micelles via the simultaneous reduction of equimolar concentrations (10^{-3} M) of $PtCl_4$ and $Co(AOT)_2$. The water content $W = [H_2O]/[AOT]$ is 10 leading to a micellar diameter of 3 nm. Sodium tetrahydroboride, $NaBH_4$, is used in large excess (10^{-2} M) as a reducing agent. Immediately after borohydride addition, the micellar solution color turns from dark yellow to black, indicating the formation of colloidal par-

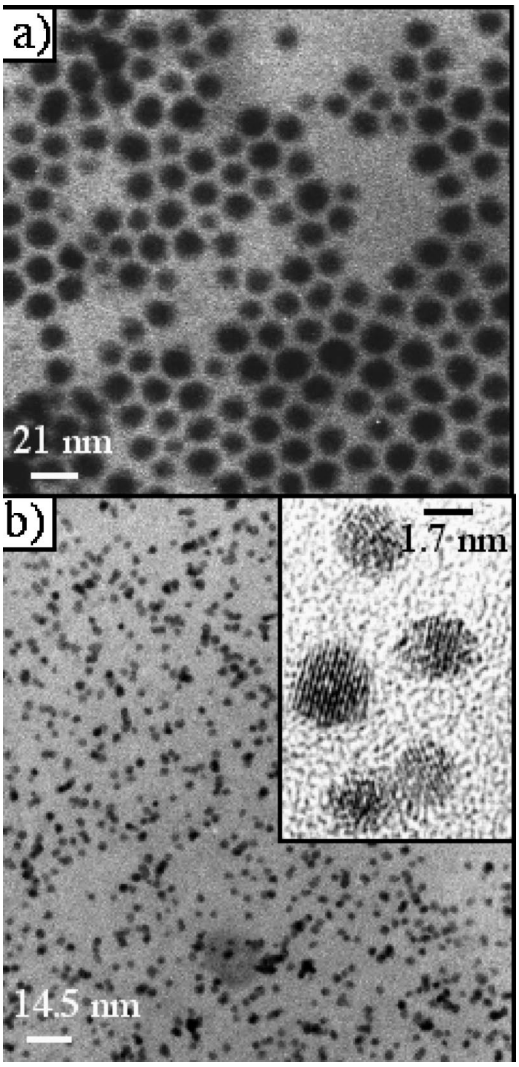

FIG. 1. (A) TEM micrograph of monolayer film made of 7-nm-diam cobalt nanocrystals. (B) TEM micrograph of monolayer film made of 2.7-nm-diam $Co_{53}Pt_{47}$ nanocrystals. The inset is a HRTEM picture showing the lattice fringes of CoPt in the disordered fcc structure. The interlattice distance is 2.12 Å.

ticles. Dodecylamine, $C_{12}H_{25}NH_2$, added to the micellar solution, complexes the metal atoms at the surface of the nanocrystals. The coated cobalt–platinum nanocrystals are then extracted from the reverse micelles by ethanol addition and dodecylamine-coated nanocrystals are precipitated. The particles are then washed and centrifuged several times with ethanol to remove all the surfactant. A black powder is obtained, which can be easily redispersed in a solvent like hexane. These nanocrystals have been characterized by TEM and energy dispersive x-ray (EDX) analysis [Table I and Fig. 1(B)]. Their average size is 2.7 nm and they have a relatively large size polydispersity ($\sigma = 24\%$ for the diameter distribution). The elemental composition obtained from EDX analysis is $Co_{53}Pt_{47}$, which is consistent with the equimolar solutions used for the reduction. The as-prepared CoPt are crystalline nanoparticles as evidenced by clearly resolved lattice fringes in high-resolution transmission electron microscopy (HRTEM) [Inset Fig. 1(B)]. The selected area electron diffraction pattern is similar to that of the platinum, which indicates the formation of the chemically disordered face-centered-cubic (fcc) CoPt structure. Nanophase segregation cannot be totally excluded from these data. However, we have further evidence excluding segregation. Domains of pure Co have a lower contrast in TEM than those of Pt or CoPt,[35] thus Co domains should be distinguishable from domains of Pt and CoPt. However, we observe homogeneous contrast in the TEM images and no core shell structure by HRTEM [inset Fig. 1(B)]. The interlattice distance is 2.12 Å. It is 2.05 for bulk cobalt fcc (111) and 2.27 Å for bulk platinum fcc (111). It is known that the CoPt bulk alloy forms a complete solid solution.[36] Thus assuming that Vegard's law has a linear dependency between $Co(111)_{fcc}$ and $Pt(111)_{fcc}$ planes, the $CoPt(111)_{fcc}$ atomic spacing at a Pt concentration of 47% is estimated to be 2.15 Å, which is close to the measured d spacing of 2.12 Å. This confirms the formation of $Co_{53}Pt_{47}$ and suggests negligible Pt surface segregation. In addition, the elemental composition obtained after extraction is close to the initial one of the salt. This constant stoichiometry, as well as the TEM and diffraction results, rule out the possibility of nanophase segregation or core-shell formation.

IV. MAGNETIC MEASUREMENTS AND ANALYSIS

A. Blocking temperature

Our MOKE investigation is similar to a zero field cooled experiment. The sample is cooled down to 50 K without applied field starting from a temperature where all the particles are in the superparamagnetic. Afterwards, the initial susceptibility, χ_0 as function of the increasing temperature is measured as the field derivative, at zero field of the Kerr intensity with the external field sweeping at a frequency of about $f = 0.1$ Hz in a ± 100 Oe range.

In the case of an ideal system of perfectly monodisperse particles, the temperature T_b at which the susceptibility peak occurs represents the particle blocking temperature which is related to the particle magnetic anisotropy energy KV by the relation $KV = k_B T_B \ln(1/f\tau_0) \approx 28\, k_B T_B$, where V is the particle volume, K is the magnetic anisotropy energy (MAE) per volume unit and $\tau_0 \approx 10^{-9} - 10^{-11}$ s.[37] In the case of a system of polydisperse particles, the volume V has to be replaced by an effective volume V_{eff} proportional to the average volume, $V_{\text{eff}} = \langle V^2 \rangle / \langle V \rangle$.[38]

TABLE I. Size and polydispersity of the nanocrystals depending on the annealing temperature.

Nanocrystals	Co (RT)	Co (550 K)	CoPt (RT)	CoPt (370 K)	CoPt (700 K)	CoPt (800 K)
Diameter (nm)	7	6.5	2.8	2.7	3.4	3.1
Polydispersity (%)	15	17	24	21	34	31

B. Superparamagnetic Curie temperature, T_0

In a weak applied field, and in the absence of interactions, an assembly of superparamagnetic particles obeys to a Curie-like law, $\chi_0 = C/T$. In a dense system, due to the dipolar interactions, the effect of the demagnetizing field has to be taken into account.[39] In the continuum limit, the effective field acting on a volume element containing one particle can be expressed, in the superparamagnetic regime, as

$$H_{\text{eff}} = H_0 - N_e M_v + H_{\text{lor}}, \tag{1}$$

where N_e is the demagnetizing factor along the direction of the applied field H_0, corresponding to the external shape of the sample, M_v is the magnetization per volume unit, and H_{lor} is the Lorentz field ($H_{\text{lor}} = N_i M_v$ with $N_i = 4\pi/3$). Consequently, the initial susceptibility becomes $\chi_0 = C/[T + C(N_e - 4\pi/3)]$. By using the usual expression $\chi_0 = C/(T - T_0)$, an order temperature T_0 is defined

$$T_0 = -C(N_e - 4\pi/3). \tag{2}$$

T_0 characterizes the effect of magnetostatic interactions.[40] By analogy to paramagnetism T_0 is also called the superparamagnetic Curie temperature.[39] Equation (2) implies that films with the same chemical composition can be characterized by different ordering temperatures, depending on the film morphology and the geometry of the experiments. For example, in the case of a homogeneous structure less thin film, $N_e = 0$ when the field is applied parallel to the sample plane and $N_e = 4\pi$ when the field is applied perpendicular to the sample plane. As a consequence, the ordering temperature varies markedly: $T_0^{\text{para}} = C \times 4\pi/3 > 0$ (ferromagnetic-like interaction) for H parallel to the film plane or $T_0^{\text{perp}} = -C \times 8\pi/3 < 0$ (antiferromagnetic-like interaction) for H perpendicular to the film plane.

V. RESULTS AND DISCUSSION

A. Nanocrystal films grown in an external magnetic field

The topological and magnetic properties of films grown in an external magnetic field were addressed by means of atomic force microscopy (AFM) and MOKE. This part is restricted to pure cobalt nanocrystals since for the as-prepared CoPt alloy nanocrystals there was no detectable effect of an external field applied during deposition. We attribute this to the low magnetic response, at room temperature, of the much smaller CoPt nanocrystals. Co nanocrystals are dispersed in hexane and their concentration is fixed at 5×10^{-7} M. A HOPG substrate is placed at the bottom of a cell containing 200 μl solution. In the following, we consider three samples of cobalt nanocrystals fabricated by applying different magnetic fields during deposition.

(i) Without applied field, a monolayer of uncoalesced cobalt nanocrystals is formed [Fig. 2(A)]. Large areas (50 μm^2 on average) covered by a continuous film of nanocrystals are distributed on the overall substrate. We also observe that cobalt nanocrystals align themselves along the atomic steps of the HOPG substrate. This phenomenon is usually seen with clusters formed by electron beam evaporation.[41] It results from diffusion of the clusters on the substrate after their deposition. The monolayer height is 10 nm [Fig. 2(D)], which corresponds to the size of the nanoparticles coated by the dodecylamine (9 ± 1 nm). The lateral diameter (20 nm) of the nanoparticles is overestimated, due to tip convolution.[42] This monolayer, obtained without a deposition field, is called sample A.

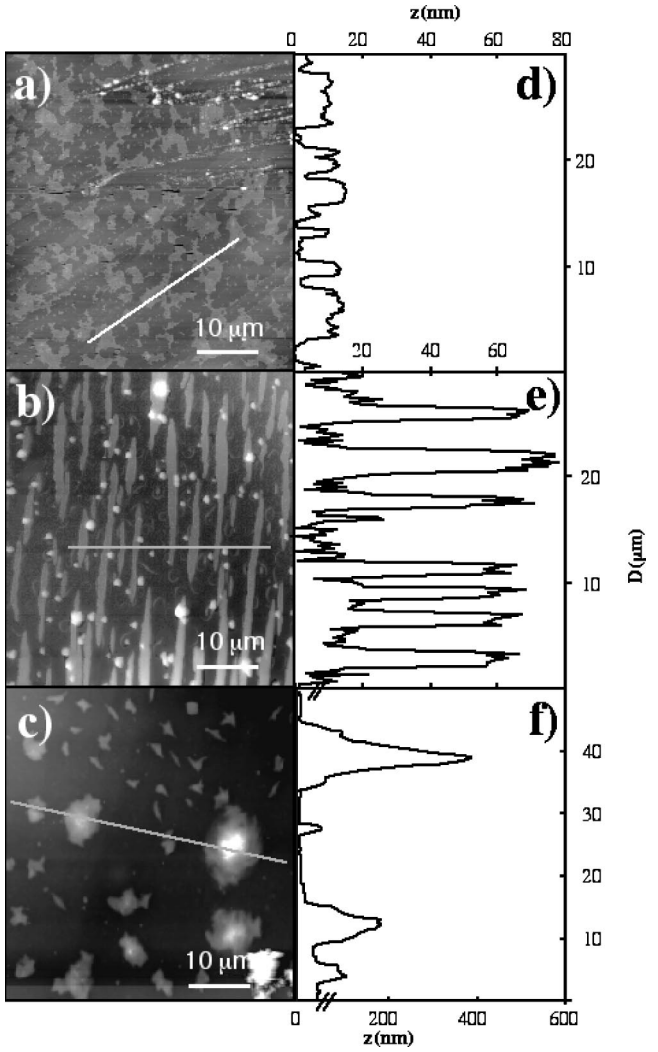

FIG. 2. AFM images (50×50 μm^2) of films of uncoalesced cobalt nanocrystals deposited on HOPG (A) without a magnetic field, (B) in a magnetic field (0.3 T) parallel to the substrate, and (C) in a magnetic field (0.3 T) perpendicular to the substrate. (D, E, F) are z profiles taken as indicated in the top view images.

(ii) Figure 2(B) shows stripes made of uncoalesced cobalt nanocrystals on the HOPG substrates obtained by applying a magnetic field (0.3 T) parallel to the substrate. The average stripe length and height are 30 μm and 60 nm, respectively, corresponding to the stacking of six layers of coated nanocrystals [Fig. 2(E)]. The interstripe distance is about 5 μm, in agreement with our previous results.[10,11] This sample, obtained in a parallel magnetic field, is called sample B.

(iii) When the magnetic field (0.3 T) is applied perpendicular to the substrate, the film appears more chaotic [Fig. 2(C)]. Nanocrystals pile up into 50–400 nm high peaks with mean diameter of about 5 μm [Fig. 2(F)]. This sample, obtained in a perpendicular magnetic field, is called sample C.

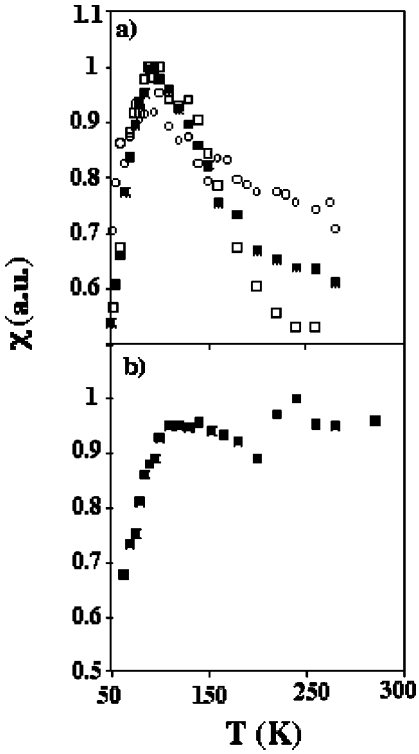

FIG. 3. (A) Temperature dependence of the initial susceptibility, χ_0, for a film deposited without external magnetic field (open circles), deposited in a magnetic field parallel to the substrate (solid squares), and deposited in a magnetic field perpendicular to the substrate (open squares). (B) Temperature dependence of χ_0 for cobalt nanocrystals deposited with a magnetic field parallel to the substrate and annealed *in situ* at 500 K for 10 min.

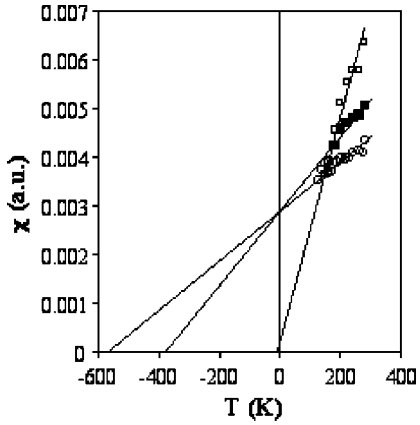

FIG. 4. Plots of χ_0^{-1} with T (K) in the superparamagnetic regime. [Symbols as in Fig. 3(A)].

The magnetism of these samples was addressed by recording the temperature dependence of the initial susceptibility, χ_0 [Fig. 3(A)]. As expected, a maximum is observed corresponding to the transition from the blocked state, at low temperature, to the superparamagnetic state, at the higher temperatures.

For sample A, we measured $T_b = 90 \pm 5$ K. A similar value, $T_b = 85$ K, was obtained by SQUID experiments.[10] From the size distribution evaluated by TEM we estimated $V_{\text{eff}} = 1.8\ V_{\text{mean}}$, giving $K = 1.1 \times 10^6$ erg/cm^3, close to previous values measured for ε-Co and mt-fcc Co particles.[43] For samples B and C, T_b is slightly higher and equal to 100 ± 5 K. Since the particles are identical to the case A, this increase in the peak temperature is clearly ascribed to the different film structures induced by applying an external magnetic field during deposition. The shape anisotropy of a structured film differs from that of a homogeneous flat film. Moreover, dipolar interactions can be affected by a possible partial alignment of the particle easy axes induced by the external field.

A similar effect was observed for 12 nm fcc Co particles deposited by applying a field of 0.35 T in the film plane.[44] The authors observed an in-plane uniaxial anisotropy with an anisotropy field $H_{\text{an}} = 0.037$ T. The anisotropy field is related to the particle MAE by $KV = H_{\text{an}}\mu/2$ where μ is the particle magnetic moment. Assuming a bulk-like magnetic moment for the Co atoms ($\mu_{\text{co}} \approx 1.8\ \mu_B$), and a similar anisotropy field, we find a supplementary anisotropy of $K = 5 \times 10^4$ erg/cm^3, which corresponds to an increase of about 5 K in the blocking temperature of the striped film.

The second parameter which can be derived from by the χ_0 vs T curves is the ordering temperature, T_0, which is a measure of the interparticle interactions.[39,40]

Experimentally T_0 is deduced from the linear variation of χ_0^{-1} with T in the superparamagnetic regime (Fig. 4). It drastically differs for the three samples. For sample A, T_0 is -550 ± 50 K. This large negative value of the ordering temperature might at first glance be interpreted as antiferromagnetic order in the monolayer. However, we find for the same samples in a SQUID magnetometer, where the field is parallel to the sample plane, $T_0 = 50$ K, which corresponds to ferromagnetic order. As shown above, this result can be explained in terms of the demagnetizing field. Sample A can be considered as a homogeneous thin film. Thus, depending on the geometry of the experiment, the demagnetizing field changes. The negative value of T_0 obtained from MOKE measurements ($T_0 = -550$ K) is qualitatively consistent with formula (2), for the case of the field applied perpendicular to the sample ($N_e = 4\pi$). On the other hand, in our SQUID experiment the magnetic field is applied parallel to the sample ($N_e = 0$) and then a positive value for T_0 is expected. The large negative value of T_0 found by MOKE experiments is in good agreement with recent calculations of the susceptibility of superparamagnetic interacting cobalt nanoparticles.[40] The authors calculated $T_0 = -150$ K for a film of unorganized 7-nm-diam cobalt nanocrystals with a packing density of 20% and showed a linear dependence of T_0 with the packing density. Our sample shows large areas with a continuous monolayer [Fig. 2(A)]. Inside these areas each nanocrystal feels a dipolar field that can be considered as due to a homogeneous film with a close to compact organization (i.e., 74%). This yields an ordering temperature $T_0 = -555$ K, which compares well with the experimental value, $T_0 = -550$ K. Our data gives -11 for the ratio $T_0^{\text{perp}}/T_0^{\text{para}}$ instead of -2, predicted by Eq. (2). There are few experimental results allowing a comparison with the theoretical variation of T_0. However, in the case of interacting small Fe/Al_2O_3 particles, $T_0 = 25$ K is found in the parallel case and $T_0 = -130$ K in the perpendicular one (i.e., a ratio

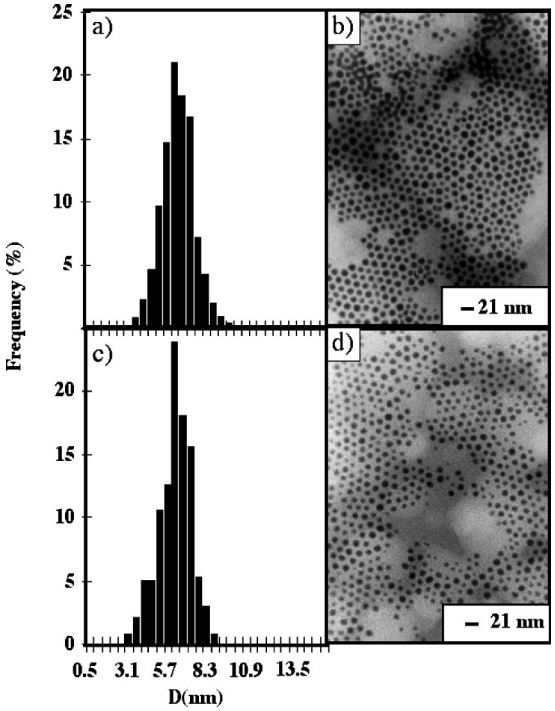

FIG. 5. Size histogram and corresponding TEM picture for cobalt nanocrystals deposited on a TEM grid coated with amorphous carbon at room temperature (A and B) and after annealing for 10 min at 550 K (C and D).

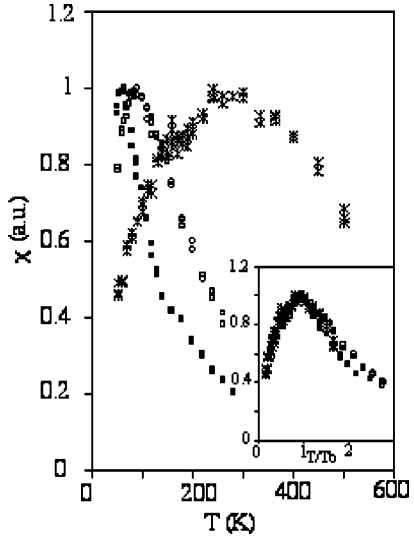

FIG. 6. Temperature dependence of the initial susceptibility, χ_0, for CoPt nanocrystals deposited on HOPG substrates and annealed *in situ* for 10 min. Sample annealed at 700 K (solid square), sample annealed at 800 K (open circle), and sample annealed at 950 K (stars). The inset shows the normalized susceptibility vs T/T_b.

of -5).[45] This discrepancy with theory is probably due to the continuum assumption of the model used for the determination of T_0.[39]

The effect of the demagnetizing field can also explain the large variation of the ordering temperature observed for samples B and C.

For sample B, $T_0 = -350 \pm 50$ K. The AFM image [Fig. 2(B)] reveals the presence of stripes, which can be considered as elongated ellipsoids. In this case the demagnetizing factor N_e is 2π if the field is applied perpendicular to the stripes and to the film plane. Equation (2) gives $T_0 = -C \times 2\pi/3 < 0$. T_0 is negative and expected to decrease by a factor of 4 compared to sample A. The experiment shows again good qualitative agreement, however the decrease is only a factor 1.6.

For sample C, $T_0 = 0 \pm 10$ K. Assuming a perpendicular orientation of the dot easy axis following the deposition in the external field, the demagnetizing factor N_e is 0 and then $T_0 = C \times 4\pi/3 > 0$. On the other hand, for large spherical and isolated aggregates, the demagnetizing factor is $4\pi/3$ and $T_0 = 0$. Thus, T_0 is expected to be 0 or positive, in agreement with the experimental result.

B. Annealing of cobalt nanocrystals

Figure 3(B) shows the drastic change in the temperature dependence of χ_0 when the sample B is annealed *in situ* at 500 K for 10 min. χ_0 increases as in the nonannealed case, then it takes on an almost constant value between 100 and 320 K, indicating a room temperature ferromagnetic behavior. This cannot be attributed to coalescence of the nanocrystals during the annealing process. A TEM investigation of a cobalt monolayer annealed under the same conditions shows that both the structure and the average size do not change during *fast* annealing (Fig. 5). Similarly, AFM images exclude modifications in the film topography. Our results are consistent with those reported by Wang *et al.*[30,46] on the annealing of metallic nanocrystals with similar sizes. Indeed, annealing, increasing the crystallographic order or inducing a phase transition in the nanocrystals, markedly improves the magnetic properties of uncoalesced cobalt nanocrystals. The plateau observed in the χ_0 vs T curve can be attributed to an incomplete crystallographic transformation of the particle structure, due to a too low annealing temperature or a too short annealing time. In that case a large MAE dispersion is expected due to the coexistence of particles in the soft and in the hard magnetic phase. Figure 3(B) tends to confirm this assumption. Looking in detail to the χ_0 vs T curve we can note that the plateau can be explained as the superposition of two distinct peaks centered at about 120 and 250 K, respectively. Assuming two types of nanocrystals having the same size distribution in the film, their magnetic anisotropy energy could be evaluated to 2.1×10^6 and 4.4×10^6 erg/cm^3, respectively. These values are close to the bulk values of the fcc structure (2.5×10^6 erg/cm^3) and hcp structure (4.5×10^6 erg/cm^3).[47] Murray and Sun,[48] report such a change from the ε phase to the hcp phase for 9 nm cobalt nanocrystals heated at 570 K. However, in our case the cobalt nanocrystals are ferromagnetic at room temperature after annealing at 500 K and they still keep the mesoscopic film structure without coalescence.

C. Annealing of CoPt nanocrystals

CoPt nanocrystals obtained by soft chemistry in colloidal assemblies are in the disordered fcc phase. SQUID measurements show a blocking temperature of 5 K for the as-prepared 2.7 nm $Co_{53}Pt_{47}$ nanocrystals. The blocking

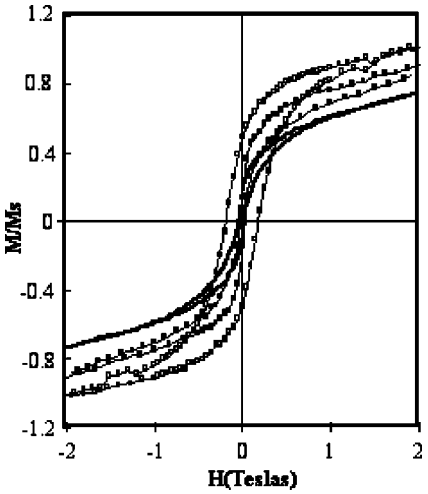

FIG. 7. Hysteresis loops of CoPt nanocrystals (solid line) at 3 K for the as-prepared CoPt nanocrystals, (open squares) at 3 K for CoPt annealed at 950 K, (solid circles) at 300 K for CoPt annealed at 950 K.

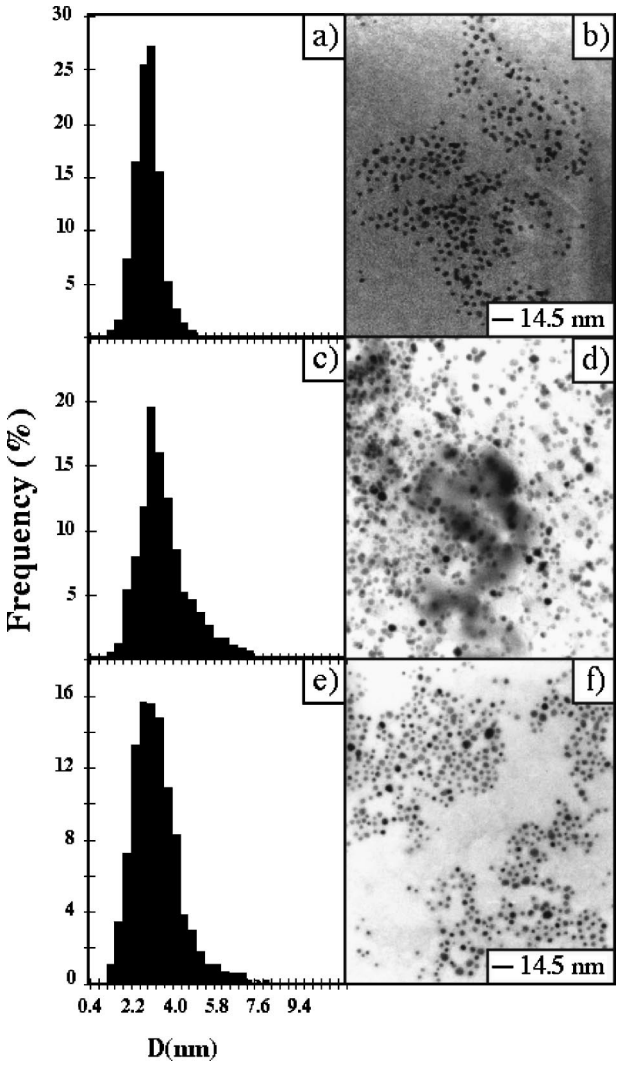

FIG. 8. Size histograms and corresponding TEM images for CoPt nanocrystals deposited on a HOPG sheet glued on a TEM grid: (A and B) after annealing for 1 h at 370 K, (C and D) after annealing for 10 min at 700 K, and (E and F) after annealing for 10 min at 800 K.

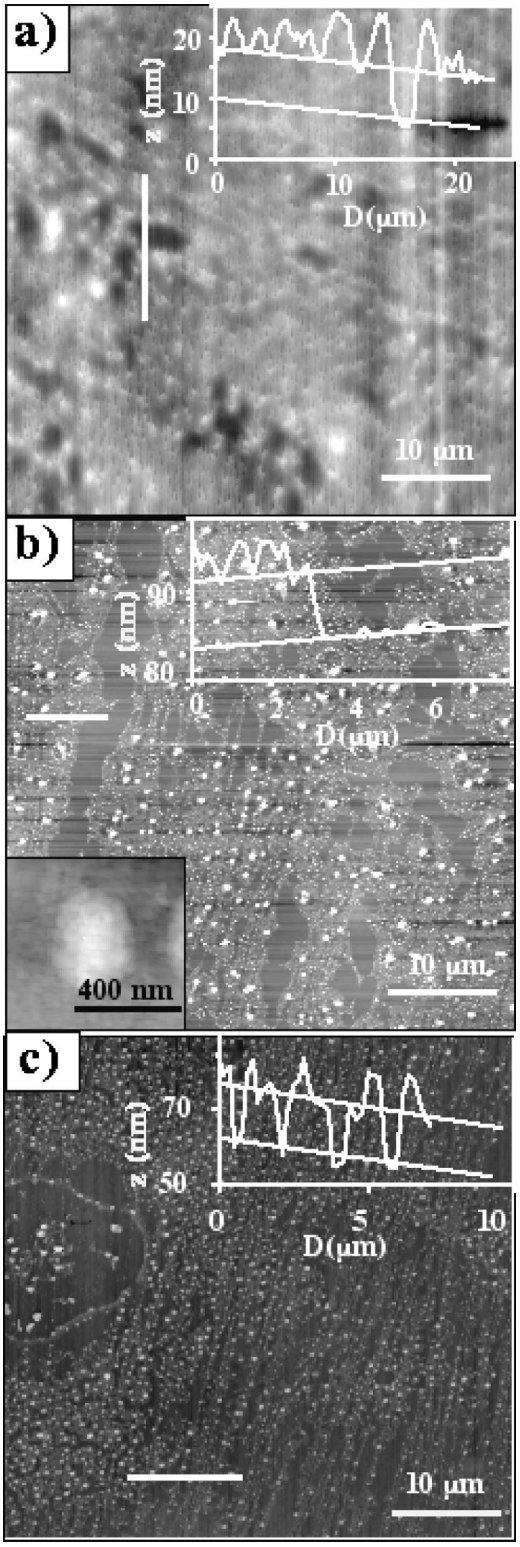

FIG. 9. AFM image ($50\times50\ \mu m^2$) of film made of CoPt nanocrystals deposited on HOPG: (A) annealed at 370 K for 1 h, (B) annealed at 700 K for 10 min, (C) annealed at 800 K for 10 min. (Inset B is a magnification on the spherical aggregates: they are made of uncoalesced nanocrystals.)

temperature undergoes a large variation with the annealing temperature (Fig. 6). From the temperature dependence of the initial susceptibility, measured by polar MOKE, we find $T_b<50$ K for the as-prepared nanocrystals heated at 370 K during the sample preparation, $T_b=60$ K after *fast* annealing

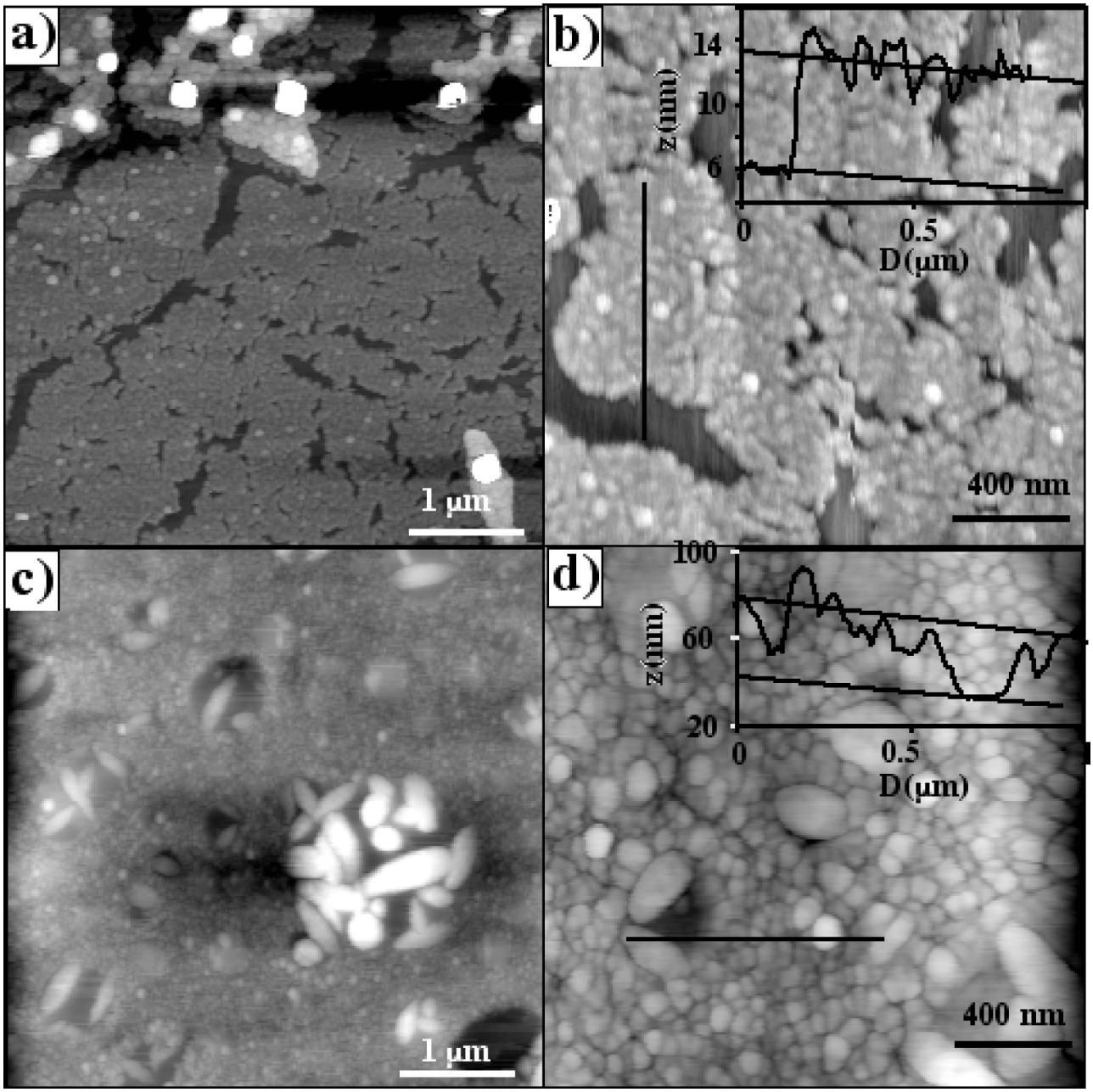

FIG. 10. AFM images of films made of CoPt nanocrystals deposited on HOPG: (A and B) annealed at 800 K for 10 min, and (C and D) annealed at 950 K for 10 min. Insets are the corresponding *z* profiles taken along of the lines indicated in Figs. B and D.

to 700 K, $T_b = 100$ K after *fast* annealing to 800 K, and $T_b = 280$ K after *fast* annealing to 950 K. A similar evolution toward a room temperature ferromagnetic state is also observed in the hysteresis loops measured by SQUID (Fig. 7). A coercive field of about 300 Oe is measured at room temperature for the particles annealed to 950 K. Saturation is not reached even at 3 T for the as-prepared CoPt nanocrystals, but it is reached at 2 T after annealing. The reduced remanence, M_r/M_s, and the coercivity markedly increase from 0.2 to 0.5 and 250 to 2000 Oe after annealing, respectively. Inversely, the ordering temperature does not change with annealing and stays constant at $T_0 = 40 \pm 4$ K, suggesting a weak ferromagnetic coupling independent of the annealing temperature.

A similar annealing induced transition from a superparamagnetic to a ferromagnetic room temperature state was recently observed in $Co_{50}Pt_{50}$ nanocrystals with a slightly larger diameter of about 4 nm.[49] This change in the particle magnetic properties was essentially explained by the face-centered-cubic to face-centered-tetragonal phase transition occurring at annealing temperatures above 820 K. Nevertheless, the authors were not able to exclude particle coalescence as a main cause of the observed increase of the particle blocking temperature. Conversely, our MOKE measurements bear information, which can be used to exclude particle coalescence. We recall that for an ideal system of monodisperse particles the initial susceptibility drops upon cooling from the maximum at T_b to zero in a few degrees and that the

width of this transition becomes larger with increasing the size (MAE) dispersion of the particles. If coalescence takes place, we expect an increase of this transition width with the annealing temperature. Our data show that the relative peak widths of the χ_0 vs T curves remain unchanged with annealing temperature, thus suggesting the absence of coalescence (see inset Fig. 6).

The analysis of the samples by TEM and AFM confirms the absence of coalescence at least until annealed to 800 K. In the TEM data absence of coalescence manifests itself in the constant particles diameter up to $T=800$ K (Fig. 8). Higher annealing temperature is precluded to our TEM microscope. CoPt nanocrystals deposited on a sheet of HOPG glued on a TEM grid retain their spatial arrangement and crystallographic structure following annealing to 370 K for 1 h and then to 700 and 800 K under nitrogen for 10 mn. The average size and diameter dispersion slightly increase from 2.7 nm at 370 K to 3.2 nm at 800 K and from 20% to 31%, respectively (see Table I). After annealing a few larger nanocrystals appear in the size distribution (Fig. 8), probably due to Ostwald ripening as the nanocrystals can diffuse on HOPG at high temperature. However, this slight change if the size distribution is not sufficient to significantly change the MAE distribution as observed experimentally. The selected area electron diffraction reveals, at 800 K, the characteristic patterns of CoPt $L1_0$ with main rings at 3.42, 2.55, 2.18, 1.95, and 1.76 Å. This is close to the diffraction patterns of bulk CoPt. 3.60, 2.68, 2.16, 1.90, and 1.84.[50] AFM pictures indicate that the annealing induced phase transition from the disordered fcc CoPt to the ordered CoPt $L1_0$ occurs without change of the average size of the nanocrystals (Figs. 9 and 10).

The film of CoPt nanocrystals appears more ordered at 700 and 800 K than at 370 K (Fig. 10). At these temperatures, the coating agent burns, leaving a graphite shell surrounding the nanocrystals,[51] which probably favors the nanocrystals' diffusion on the HOPG substrate, but still protects them from coalescence. Due to this increased surface mobility, the nanocrystals move to decorate lines forming along the atomic steps of the substrate.[52] Due to the tip convolution it is not possible to distinguish if the nanocrystals are coalesced or not. But up to 800 K, the height of the CoPt monolayer is constant, equal to 7 ± 2 nm, which is consistent with the TEM results. At 950 K a drastic change occurs. At some locations large aggregates are observed indicating that particle coalescence takes place [Figs. 10(C) and 10(D)]. However, other locations of the film remain unchanged between 800 and 950 K. This is in good agreement with the results published by Wang *et al.*[30,46] They show the beginning of coalescence for gold and platinum nanocrystals coated by dodecanthiols above 850 K. Thus we can assume that at 950 K the coalescence is only partial or at the beginning, which can explain the apparent discrepancy between the topological and magnetic results.

Assuming absence of coalescence, the magnetocrystalline anisotropy of the CoPt nanocrystals can be deduced from the blocking temperature and the size distribution determined by TEM. By calculating an effective volume $V_{\text{eff}}=2.8\,V_{\text{mean}}$ we estimate $K=0.7\times10^6$ erg/cm^3 for as-prepared particles, $K=0.8\times10^7$ erg/cm^3 after annealing to 700 K, $K=1.3\times10^7$ erg/cm^3 after annealing to 800 K, and $K=3.8\times10^7$ erg/cm^3 after annealing to 950 K. Even if the last value is still slightly lower than the bulk value (4.9×10^7 erg/cm^3),[53] the trend of the MAE with the annealing temperature is consistent with the transition from the fcc phase to the fct $L1_0$ phase. Undoubtedly, *fast in situ* annealing allows obtaining the hard, magnetic phase of CoPt. However, in contrast to the cobalt particles presented above, higher annealing temperatures are needed for CoPt particles in order to obtain materials ferromagnetic at room temperature. In this case, the size distribution could be perturbed, which may present a drastic problem for the elaboration of magnetic devices based on nanosized particles. As we show here, the *fast* annealing process may contribute to solve this effect.

VI. CONCLUSIONS

We studied the magnetic and morphological properties of very thin films of magnetic nanocrystals deposited on a HOPG substrate. The film morphology reflects the symmetry imposed by applying an external magnetic field during growth: in-plane stripes, conic mountains, or homogeneous flat films are observed as a consequence of an external field applied in the film plane, perpendicular to it or in zero field, respectively. As a consequence of dipolar interactions, the film magnetism changes depending on the growth conditions. *Fast in situ* annealing was used to induce transitions in the crystallographic particle structure, while avoiding coalescence. Room temperature ferromagnetic behavior was observed in film of uncoalesced Co and CoPt particles after annealing to 500 and 950 K, respectively.

ACKNOWLEDGMENTS

The authors would like to express their gratitude to Professor M. P. Pileni and Dr. P. Bonville for fruitfull discussions. The authors thank Dr. E. Vincent and Dr. G. Lebras, DRECAM/SPEC, CEA Saclay, for the use of their SQUID equipment.

[1] See, for example, J. L. Dormann and D. Fiorani, in *Magnetic Properties of Fine Particles* (North-Holland, Amsterdam, 1992).
[2] S. A. M. Tofail, I. Z. Rahman, and M. A. Rahman, Appl. Organomet. Chem. **15**, 373 (2001).
[3] D. N. Lambeth, E. M. T. Velu, G. H. Bellesis, L. L. Lee, and D. E. Laughlin, J. Appl. Phys. **79**, 4496 (1996).
[4] C. Petit, A. Taleb, and M. P. Pileni, J. Phys. Chem. B **103**, 805 (1999).
[5] M. Hillgendorf, B. Tesche, and M. Giersig, Aust. J. Chem. **54**, 497 (2001).
[6] B. Murray, S. Sun, W. Gaschler, H. Doyle, T. A. Betley, and C. R. Kagan, IBM J. Res. Dev. **45**, 47 (2001).
[7] J. P. Chen, C. M. Sorensen, K. J. Klabunde, and G. C. Hadjipanayis, Phys. Rev. B **51**, 11527 (1995).
[8] C. Petit, A. Taleb, and M. P. Pileni, Adv. Mater. (Weinheim, Ger.) **10**, 259 (1998).
[9] V. Russier, C. Petit, J. Legrand, and M. P. Pileni, Phys. Rev. B **62**, 3910 (2000).
[10] J. Legrand, C. Petit, and M. P. Pileni, J. Phys. Chem. B **105**, 5643 (2001).
[11] C. Petit, J. Legrand, V. Russier, and M. P. Pileni, J. Appl. Phys. **91**, 1502 (2002).
[12] V. Russier, C. Petit, and M. P. Pileni, J. Appl. Phys. **93**, 10001 (2003).
[13] J. L. Dormann, D. Fiorani, F. Giammaria, and F. Lucari, J. Appl. Phys. **69**, 5130 (1991).

[14] Z. S. Jiang, G. J. Jin, J. T. Ji, H. Sang, Y. W. Du, S. M. Zhou, Y. D. Wang, and L. Y. Chen, J. Appl. Phys. **78**, 439 (1995).
[15] V. G. Kravets, A. K. Petford-Long, and A. F. Kravets, J. Appl. Phys. **87**, 1762 (2000).
[16] J. L. Menendez, B. Bescos, G. Armelles, R. Serna, J. Gonzalo, R. Doole, and A. K. Petford-Long, Phys. Rev. B **65**, 205413 (2002).
[17] B. Kalska, J. J. Pagel, P. Fumagalli, M. Hillgendorf, and M. Giersig, J. Appl. Phys. **93**, 7481 (2002).
[18] S. Sun, C. B. Murray, D. Weller, L. Folks, and A. Moser, Science **287**, 1989 (2000).
[19] B. Stahl *et al.*, Adv. Mater. (Weinheim, Ger.) **14**, 24 (2002).
[20] M. Chen and D. E. Nikles, J. Appl. Phys. **91**, 8477 (2002).
[21] J. A. Christodoulides, Y. Zhang, G. C. Hadjipanayis, and C. Fountzoulas, IEEE Trans. Magn. **36**, 2333 (2000).
[22] M. P. Pileni, Langmuir **13**, 3266 (1997).
[23] M. P. Pileni, Ber. Bunsenges. Phys. Chem. **101**, 1578 (1997).
[24] M. P. Pileni, J. Phys. Chem. B **105**, 3358 (2001).
[25] A. Kumbhar, L. Spinu, F. Agnoli, K.-Y. Wang, W. Zhou, and C. J. O'Connor, IEEE Trans. Magn. **37**, 2216 (2001).
[26] L. Yiping, Z. X. Tang, G. C. Hadjipanayis, C. M. Sorensen, and K. J. Klabunde, IEEE Trans. Magn. **29**, 2646 (1993).
[27] E. E. Carpenter, C. T. Seip, and C. J. O'Connor, J. Appl. Phys. **85**, 5184 (1999).
[28] B. Stahl *et al.*, Adv. Mater. (Weinheim, Ger.) **14**, 24 (2002).
[29] M. Chen and D. E. Nikles, J. Appl. Phys. **91**, 8477 (2002).
[30] Z. R. Dai, S. Sun, and Z. L. Wang, Surf. Sci. **505**, 325 (2002).
[31] E. Shevshenko, A. Kornowski, D. Talapin, F. Wiekhorst, J. Kötzler, M. Haase, A. Rogach, and H. Weller, Adv. Mater. (Weinheim, Ger.) **14**, 287 (2002).
[32] I. Lisiecki, P. A. Albouy, and M. P. Pileni, Adv. Mater. (Weinheim, Ger.) **15**, 712 (2003).
[33] M. L. Plumer, J. V. Ek, and D. Weller, *The Physics of Ultra-High-Density Magnetic Recording* (Springer, Berlin, 2001).
[34] J. Legrand, C. Petit, D. Bazin, and M. P. Pileni, Appl. Surf. Sci. **164**, 186 (2000).
[35] E. V. Shevchenko, D. L. Talapin, A. L. Rogach, A. Kornowski, M. Haase, and H. Weller, JACS published on the web (2003).
[36] A. S. Darling, Platinum Met. Rev. **7**, 96 (1963).
[37] L. Neel, Ann. Geophys. (C.N.R.S.) **5**, 99 (1949).
[38] J. L. Dormann, F. D'Orazio, F. Lucari, E. Tronc, P. Prené, J. P. Lolivet, D. Fiorani, R. Cherkaoui, and M. Noguès, Phys. Rev. B **53**, 14291 (1996).
[39] J. L. Dormann, D. Fiorani, and E. Tronc, Adv. Chem. Phys. **XC-VIII**, 283 (1997).
[40] R. W. Chantrell, N. Walmsley, J. Gore, and M. Maylin, Phys. Rev. B **63**, 024410 (2000).
[41] S. Padovani, P. Molinas-Mata, F. Scheurer, and J. P. Bucher, Appl. Phys. A: Mater. Sci. Process. **66**, S1199 (1998).
[42] Z. Gai, B. Wu, J. P. Pierce, G. A. Farnan, D. Shu, M. Wang, Z. Zhang, and J. Shen, Phys. Rev. Lett. **89**, 235502 (2002).
[43] G. A. Held, G. Grinstein, H. Doyle, S. Sun, and C. B. Murray, Phys. Rev. B **64**, 012408 (2001).
[44] M. Spasova, U. Wiedwald, R. Ramchal, M. Farle, M. Hilgendorff, and M. Giersig, J. Magn. Magn. Mater. **240**, 40 (2002).
[45] M. Godinho, J. L. Dormann, M. Noguès, P. Prené, E. Tronc, and J. P. Jolivet, J. Magn. Magn. Mater. **140–144**, 369 (1995).
[46] Z. L. Wang, J. M. Petroski, T. C. Green, and M. A. El-Sayed, J. Phys. Chem. B **102**, 6145 (1998).
[47] F. Luis, J. M. Torres, L. M. Garcia, J. Bartolomé, J. Stankiewicz, F. Petroff, F. Fettar, J. L. Maurice, and A. Vaurés, Phys. Rev. B **65**, 094409 (2002).
[48] S. Sun and C. B. Murray, J. Appl. Phys. **85**, 4325 (1999).
[49] A. C. C. Yu, M. Mizuno, Y. Sasaki, and H. Kondo, Appl. Phys. Lett. **81**, 3768 (2002).
[50] ASTM File 29–498.
[51] I. Lisiecki, H. Sack-Kongehl, K. Weiss, J. Urban, and M. P. Pileni, Langmuir **16**, 8802 (2000); **16**, 8807 (2000).
[52] G. M. Francis, L. Kuipers, J. R. A. Cleaver, and R. E. Palmer, J. Appl. Phys. **79**, 2942 (1996).
[53] D. Weller, A. Moser, L. Folks, M. E. Best, W. Lee, M. F. Toney, M. Schwickert, J. U. Thiele, and F. M. Doerner, IEEE Trans. Magn. **36**, 10 (2000).